Materials Today Communications 38 (2024) 107747

Contents lists available at ScienceDirect

Materials Today Communications

journal homepage: www.elsevier.com/locate/mtcomm

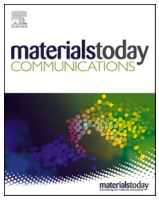

Microstructure and electrical contact properties of Al_2O_3-Cu/(Cr, Zr) composites

Heng Li [a], Meng Zhou [a,b,*], Baohong Tian [a,b,*], Yi Zhang [a,b,*], Zipeng Ma [a], Xu Li [c], Jin Zou [d], Haoyan Hu [a], Ke Jing [a], Yong Liu [a,b], Alex A. Volinsky [e]

[a] School of Materials Science and Engineering, Henan University of Science and Technology, Provincial and Ministerial Co-construction of Collaborative Innovation Center for Non-ferrous Metals New Materials and Advanced Processing Technology, Luoyang 471023, PR China
[b] Henan Province Key Laboratory of Nonferrous Materials Science and Processing Technology, Luoyang 471023, PR China
[c] Center for Advanced Measurement Science, National Institute of Metrology, Beijing 100029, PR China
[d] Jiangxi Key Laboratory for Advanced Copper and Tungsten Materials, Jiangxi Academy of Sciences, Nanchang 330096, PR China
[e] Department of Mechanical Engineering, University of South Florida, 4202 E. Fowler Ave. ENG 030, Tampa 33620, USA

ARTICLE INFO

Keywords:
Metal matrix composites
Copper matrix composites
Fast hot press sintering
Electrical contact
Mass change
Arc erosion

ABSTRACT

Al_2O_3-Cu/25Cr1Zr and Al_2O_3-Cu/25Cr3Zr electrical contact materials were fabricated by internal oxidation and fast hot press sintering. The prepared composites have uniform dense structure with over 98% density, 40.5 IACS % and 31.8 IACS% electrical conductivity, 141 HV and 154 HV hardness. TEM results show that internal oxidation during sintering generates diffusely distributed nanoparticles of γ-Al_2O_3, pinning dislocations and strengthening the matrix. In the 25 V DC, 10–40 A electrical contact tests, Al_2O_3-Cu/25Cr1Zr and Al_2O_3-Cu/25Cr3Zr composites show an increase in anode mass and a decrease in cathode mass, with the transfer direction of the material being from cathode to anode. Under the same experimental conditions, Al_2O_3-Cu/25Cr3Zr showed superior resistance to arc erosion. With the Zr content increased from 1 wt% to 3 wt%, the mass transfer of the electrical contact material decreased by 14.2%, 28.5%, 27.2%, and 8.2%, respectively, and the average arc duration was reduced from 0.4 ms to 0.24 ms, 4.35–2.46 ms, 4.91–3.53 ms, and 5.8–4.58 ms.

1. Introduction

Metal matrix composites are materials made by combining a certain metal or its alloy as the matrix, and then adding other metal or non-metal reinforcements. Compared with pure metals, metal matrix composites have excellent comprehensive properties, not only possessing the properties of the matrix itself, but also possessing the excellent properties of various reinforcing phases [1–3]. However, due to the performance differences between each component in the material, the preparation process of metal matrix composites is relatively complex, and the preparation process has a significant impact on the material's performance [4]. Common preparation methods for metal matrix composites mainly include powder metallurgy [5], hot extrusion [6], plasma sintering [7], hot pressing [8], mechanical alloying [9,10], and in-situ growth [11]. Choosing a suitable preparation process based on the performance characteristics of various materials to obtain low-cost and excellent comprehensive performance metal matrix composite materials has always been the goal pursued by researchers.

Metal matrix composites, as a new type of material, are also widely used in the field of electrical contacts. Electrical contacts are important core components of high-voltage circuit breakers, contacts, and other components, playing an important role in making and breaking circuits, transmitting signals, and carrying current. The excellent performance of electrical contact materials has a significant impact on the reliability, stability, and service life of the overall electrical system [12,13]. When the electric contact is made and then broken, it will not only be subject to mechanical force, but also to high-temperature arc erosion, leading to fusion welding, ablation, wear and other phenomena [14]. Once the electrical contact fails during operation, it can cause accidents and serious consequences. Therefore, it is necessary to develop and prepare high-performance electrical contact materials. Silver-based composites are excellent electrical contact materials, but the high cost of silver limits their widespread applications [15]. Copper is cheaper than silver, and has excellent thermal and electrical conductivity, as well as

* Corresponding authors at: School of Materials Science and Engineering, Henan University of Science and Technology, Provincial and Ministerial Co-construction of Collaborative Innovation Center for Non-ferrous Metals New Materials and Advanced Processing Technology, Luoyang 471023, PR China.
E-mail addresses: zhoumeng0902@126.com (M. Zhou), bhtian007@163.com (B. Tian), zhshgu436@163.com (Y. Zhang).

https://doi.org/10.1016/j.mtcomm.2023.107747
Received 3 November 2023; Received in revised form 25 November 2023; Accepted 29 November 2023
Available online 1 December 2023

excellent processing properties, gradually becoming more widely used [16,17].

Among them, adding some metal oxides to the copper matrix to prepare dispersed reinforced copper matrix composites has broad research prospects for preparing good electrical contact materials [18]. Copper matrix composites with metal oxides such as Al_2O_3 [19–21], Y_2O_3 [22,23], ZrO_2 [24–26] and Cr_2O_3 [27] as the reinforced phase have been studied by researchers. The dispersion copper-based composites reinforced by Al_2O_3 nanoparticles generated through internal oxidation have excellent comprehensive performance. Al_2O_3 particles have good thermal stability, good strength and hardness at high and room temperatures, and is a good high-temperature corrosion resistant material [28,29]. Tian et al. [30] prepared Cu-0.5% Al_2O_3 composites by internal oxidation and vacuum sintering. The conductivity of the prepared composites reached 93% IACS and the softening temperature reached 800 °C. Through research on the strengthening mechanisms, it was found that nano-Al_2O_3 pinned grain boundaries and subgrain boundaries to suppress recrystallization and strengthen the matrix. Zhu et al. [31] prepared Al_2O_3-Cu/30Mo3SiC and 0.5 Y_2O_3/Al_2O_3-Cu/30Mo3SiC composites, and found that internal oxidation generated nano γ-Al_2O_3 particles dispersed in the copper matrix. The Al_2O_3 generated by internal oxidation and the added nano-Y_2O_3 particles synergically strengthen the copper matrix. These dispersed reinforcement phase particles can effectively improve the mechanical properties, strength and improve wear resistance, along with better arc erosion resistance and fusion welding performance of the composites. Li et al. [32] prepared copper matrix composites reinforced by Al_2O_3 particles by internal oxidation. The mass loss and ablation diameter of H62 copper sample are greater than the Al_2O_3-Cu composite under the same ablation current. The anchoring and protecting function of uniformly dispersed Al_2O_3 particles in the Cu matrix can improve the arc ablation performance of the composite.

In recent years, more mature copper matrix composites have been formed with Cu-W, Cu-Mo and Cu-Cr systems as the mainstream. Among them, Cu-Cr composites are considered to be the main electrical contact materials for medium-voltage high-current vacuum interrupters due to the high melting point, oxygenophilicity, hard and brittle qualities of Cr and the small solid solubility between Cu and Cr, which forms a two-phase organization of Cu and Cr at room temperature. This provides a guarantee of the closure-disconnection of the electrical contacts [33]. Inada et al. [34] found that the Cr content between 25 wt% and 35 wt% is suitable for vacuum arc interruption, and Cr content between 35 wt% and 50 wt% can be used for diffusion arc interruption. Zhu et al. [35] prepared Cu/Cr20 composite materials using spark plasma sintering and studied their morphology and mechanism after arc erosion. The study found that there are molten pools, pits, cracks, and coral-like structures distributed on the surface of the electrical contact. The material eroded by the arc was transferred from the cathode to the anode. Ag, Co, Zr and other metals can be added in the preparation of composites by powder metallurgy, along with TiB_2, SiC and other ceramic particles to further improve the mechanical properties of the composites and the resistance to arc erosion. These additions can also refine grains, so that the composite material is denser [36–39]. Camara et al. [40] prepared Cu-SiC composites and it was found that SiC could deform Cu severely, SiC particles were crushed and embedded in Cu, which refined the Cu particles, and the size of Cu particles was reduced from 23.6 nm to 21.5 nm. Guo et al. [41,42] found that TiB_2 particle size has an important effect on the mode of material transfer, and the composites with fine grain TiB_2 particles had lower mass change than with coarse TiB_2 particles. It was also found that TiB_2 particles increase the viscosity of the melt pool, which can reduce the material mass loss and erosion pits on the composite surface.

Zr has high melting point and corrosion resistance. Zr and its alloys have good high temperature stability. Cu-Zr alloys have attracted much attention because of their excellent comprehensive properties. It is found that the solubility of Zr in Cu matrix is very low at room temperature, and the precipitated CuZr phase is distributed in Cu matrix, which hinders the movement of dislocations and the migration of grain boundaries, therefore, the mechanical properties of the material can be significantly improved [43,44]. Watanabe et al. [45] investigated the effect of Zr on the properties of Cu-Cr alloys and showed that Zr formed Cu_5Zr phase in the alloys, while refining the Cr-rich phase, which improved the strength. Mahdavinejad et al. [46] prepared W/Zr/Cu electrical contact materials using powder metallurgy and found that the addition of Zr reduces the mass loss due to arc erosion and largely reduces the heat concentration and arc erosion on the surface of the electrical contacts. Yang et al. [47] found that Zr can strengthen the Cu/W interface and Cu-rich zone, and during the arc erosion process, the addition of Zr can improve the arc, which increases the arc life of the material. Deng et al. [48] prepared Cu-10Cr-0.4Zr alloys and their in-situ composites, and found that the addition of Zr can refine the grains, which can produce smaller as-cast Cr dendrites.

To sum up, in this work, we combined the advantages of the above-mentioned reinforcing phases. Two composites, Al_2O_3-Cu/25Cr1Zr and Al_2O_3-Cu/25 Cr3Zr, were designed by using Al_2O_3 dispersed Cu as matrix and adding Cr and Zr reinforcing phases. The aim is to investigate the effect of synergistic reinforcement of various reinforcing phases on the microstructure and electrical contact performance of composite materials, especially the effect of Zr content on the electrical contact performance of composite materials. Develop a copper based composite material with excellent comprehensive performance and good resistance to arc erosion. Provide reference for the design and development of low-cost copper based electrical contact materials with excellent performance.

2. Materials and methods

2.1. Preparation of composites

The original materials used in the tests include Cu-0.4 wt% Al alloy powder (purity ≥99.9%, particle size ≤25 μm), Cu_2O powder (purity ≥99.9%, average particle size 2–5 μm), Cr powder (purity ≥99.9%, particle size ≤48 μm), Zr powder (purity ≥99.9%, particle size ≤25 μm). Table 1 shows the composition ratios of the composite materials required for the experiment. The powder was proportionally weighed and poured into a ball milling jar. To avoid contamination of the powder during the mixing process, a self-made plastic ball milling tank is used. And a number of 5 mm and 3 mm diameter copper balls were added to the ball milling jar, with a ball-to-material ratio of 5:1. The mixing jar was then placed on a QQM/B lightweight ball mill to mix the powder for 6 h at a speed of 60 rpm. The mixed composite powder was placed into a round graphite mold of Φ 30 mm, and the powder was first pre-pressed with a small hydraulic machine to compact the powder in order to discharge part of the air inside. Then it was sintered by vacuum hot pressing in FHP-828 rapid hot pressing sintering furnace. The vacuum in the furnace was controlled below 10^{-2} Pa during the sintering process. First, the mold was heated to 800 °C for 8 min, and at the same time, the pressure was increased to 40 MPa for 3 min. Then, the temperature was raised to 950 °C, and the 40 MPa pressure was maintained for 15 min. Finally, cooling and depressurization started. After the temperature dropped to 550 °C and the pressure dropped to 25 MPa, the sample was taken out after cooling to room temperature in the furnace. The preparation process of the composites is shown in Fig. 1.

Table 1
Composition ratio of Al_2O_3-Cu/(Cr, Zr) composites, wt%.

Composites	Cu-0.4 wt%Al	Cu_2O	Cr	Zr
Al_2O_3-Cu/25Cr1Zr	70.48	3.52	25	1
Al_2O_3-Cu/25Cr3Zr	68.57	3.43	25	3

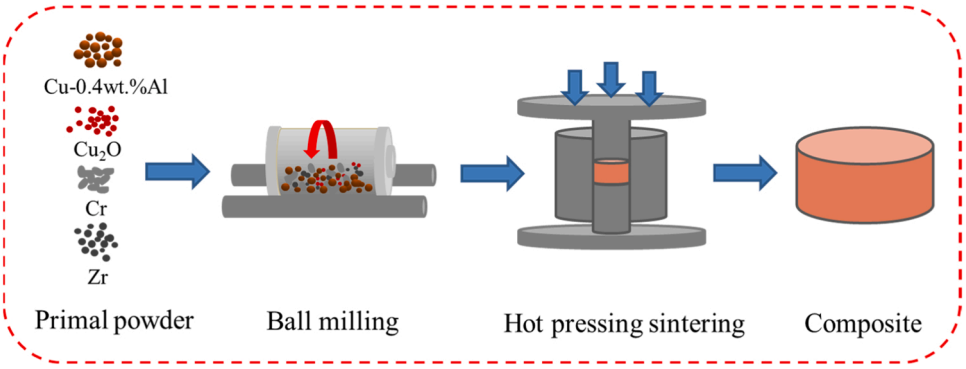

Fig. 1. Preparation process of composite materials.

2.2. Materials performance testing

Sintered Al_2O_3-Cu/(Cr, Zr) composite materials were polished with 400, 800, 1200, and 2000 mesh sandpaper on both sides using a polishing machine to remove surface oxide layers, pits, or scratches. The following performance tests were conducted using these composite materials.

The conductivity of the sintered composites was tested according to the GB/T 351–2019 conductivity test standard using a Sigma 2008B1 digital conductivity tester. In order to ensure the reliability of the data, 10 measurements were performed to find the average value.

The Vickers hardness of the sintered specimens was measured using an HVS-1000 microhardness tester at 300 gf load and 10 s loading time in accordance with the GB/T 4340–2009 Vickers hardness test standard. Each sample was measured 8 times to obtain the average value.

The actual density of the sintered state composites was tested according to GB/T 3850–2015 metal material density test standard. The dry and wet weights of sintered samples were measured using the MS304S hydrostatic balance based on the Archimedes principle. The actual density of the sintered samples was calculated using Eq. (1). In order to ensure the accuracy of the data and reduce errors, the dry weight and wet weight of the material were tested five times each to obtain the average value.

$$\rho_r = \frac{m_a}{m_a - m_b}(\rho_w - \rho_L) + \rho_L \quad (1)$$

Here, ρ_r is the actual density of the material in g/cm^3, m_a is the dry weight in g, m_b is the wet weight in g, ρ_w is the density of deionized water in g/cm^3, and ρ_L is the density of air in g/cm^3.

The sintered specimens were machined into Φ5 mm × 10 mm cylinders, and room temperature compression tests were performed using a Shimadzu AGI-250 kN universal testing machine at a compression rate of 1 mm/min, and three compression samples of each specimen were prepared for the compression tests, according to the GB/T 7314–2005 room temperature compression test standard.

2.3. Electrical contact testing

The electrical contact tests were conducted using the JF04C contact testing system. The sintered specimen was machined into a Φ3.8 mm × 10 mm cylinder as the movable and static electrical contacts of the electrical contact experiment. The upper movable contact was the anode and the lower static contact was the cathode. Before the experiment, the surface of the electrical contact was polished. The mass of the electrical contact m_1 before the test and m_2 after the test was measured using an FA2004B balance with a 0.1 mg accuracy to calculate the change in the mass of the electrical contact before and after the test Δm. The test parameters are 25 V DC, 10,000 times of making and breaking contact under 10–40 A conditions, with a frequency of 1 Hz. The closing pressure range of the electrical contact was controlled between 0.4 N and 0.6 N. The working schematic diagram of the JF04C contact testing system is shown in Fig. 2.

2.4. Microstructure characterization

The JSM-IT100 scanning electron microscope was used to observe and analyze the surface morphology of raw powder, composite powder, sintered samples, and after arc ablation. Energy-dispersive X-ray spectroscopy (EDS) analysis was performed on the sintered and arc-eroded samples using a JSM-7800 F field emission scanning electron microscope. The three-dimensional morphology of the sample surface after electrical contact was observed using a PA53MET-3D high-field optical microscope. The specimens were ion-thinned using a Gatan 695 ion miller. The microstructure of the samples was analyzed using a Zeiss LIBRA-200FE transmission electron microscope.

3. Results

3.1. Microstructure of composites

Fig. 3 shows the SEM morphology of the original powder and mixed composite powder of the Al_2O_3-Cu (Cr, Zr) composite material. The Cu-0.4 wt% Al and Cu_2O powders are spherical or ellipsoidal, while the Cr and Zr powders are lumpy particles with irregular morphology. It can be seen from Fig. 3(e) and (f) that after ball milling and mixing, the two composite powders were mixed uniformly and no powder agglomeration occurred.

In order to observe the structure morphology and distribution state of the two composites after sintering, SEM and EDS analysis was carried out on the sintered, Al_2O_3-Cu/25Cr1Zr and Al_2O_3-Cu/25Cr3Zr

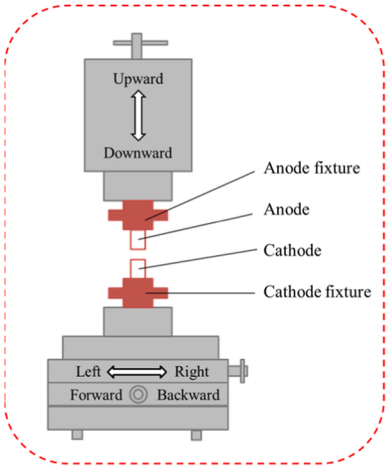

Fig. 2. Schematic diagram of the JF04C contact testing equipment.

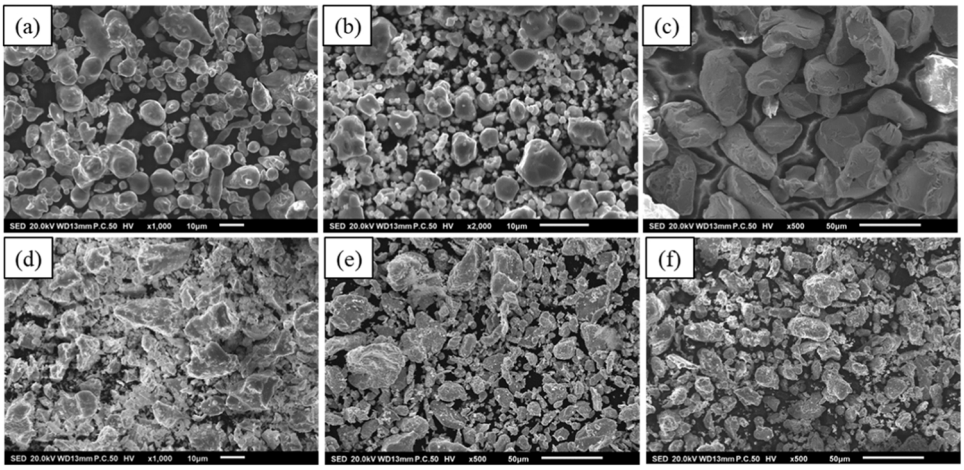

Fig. 3. SEM morphology of the original and composite powders: (a) Cu-0.4 wt%Al; (b) Cu_2O; (c) Cr; (d) Zr; (e) Al_2O_3-Cu/25Cr1Zr composite powder; (f) Al_2O_3-Cu/25Cr3Zr composite powder.

composites, as shown in Fig. 4. The structure of the prepared composites is dense, the Cr and Zr particles are uniformly distributed in the Cu matrix. The Cu matrix is gray, the large black particles are the Cr particles, and the small bright white particles are the Zr particles, and there are no obvious pore spaces or agglomeration. It can be seen from the line scan results of Cr and Zr particles in Fig. 4(e) and (f), that the dispersed copper matrix is tightly bound to Cr and Zr, and there is no oxide at the interface. The steep line scan data of Cu and Cr indicate that there is no mutual solubility between the two, while Cu and Zr form a certain solid solution.

The TEM images of the Al_2O_3-Cu/25Cr3Zr composite are shown in Fig. 5. It can be seen from Fig. 5(a) that a large number of nano particles are dispersed in the Cu matrix. and after selective area electron diffraction (SAED) and calibration (Fig. 5(b)), these nanoparticles were identified as γ-Al_2O_3 generated by internal oxidation. These γ-Al_2O_3 nano particles are diffusely distributed in the Cu matrix, pinning dislocations, increasing the resistance to dislocation motion and strengthening the matrix. W. S. Barakat et al. [49] studied the nano Ag/Cu coated nano Al_2O_3 reinforced aluminum matrix composite material and found that the in-situ generated Al_2O_3 can effectively hinder the movement of dislocations, greatly improving the strength and hardness of the material. The presence of twins in the material is also found, and the twins can hinder the dislocation movement well, thus strengthening the material. Another type of nanoscale particles was also found in the Cu matrix, whose HRTEM image is shown in Fig. 5(e). After FFT and calibration, it is determined that the nanoparticles are Cu10Zr7 phase

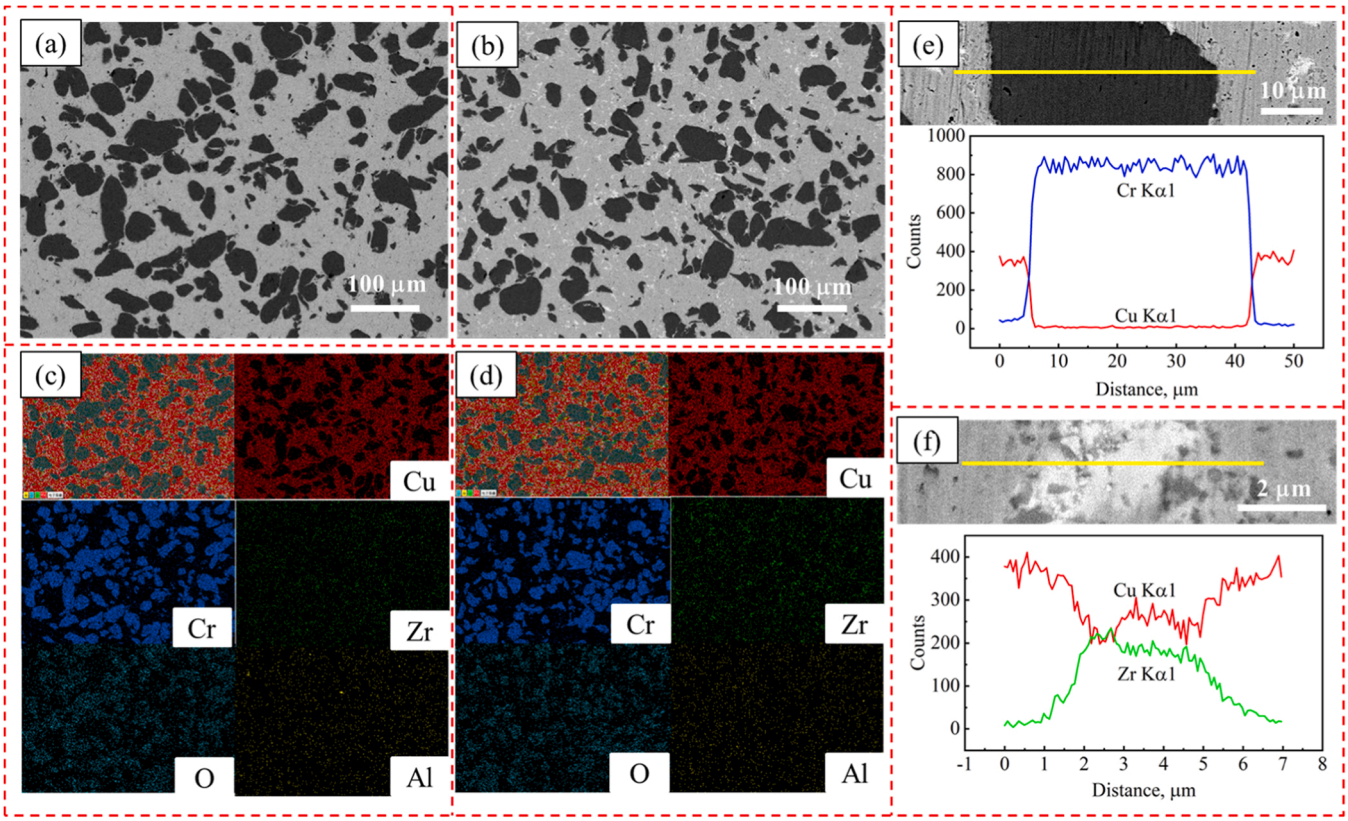

Fig. 4. SEM morphology and EDS elemental analysis of sintered composites: (a, c) Al_2O_3-Cu/25Cr1Zr; (b, d) Al_2O_3-Cu/25Cr3Zr; (e, f) EDS line scans.

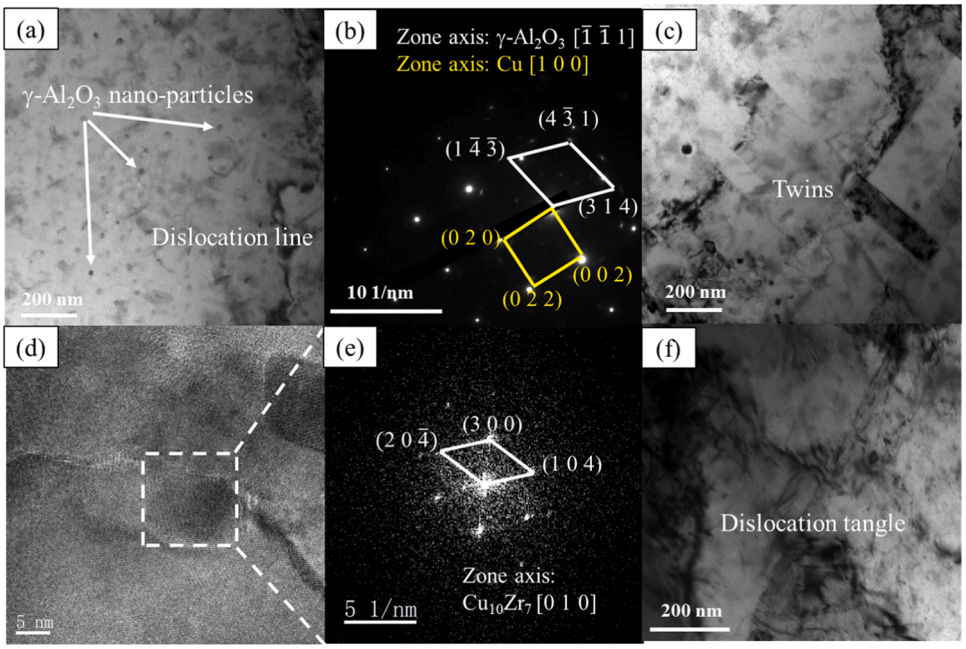

Fig. 5. TEM images of Al_2O_3-Cu/25Cr3Zr composites in sintered state. (a) Morphology of γ-Al_2O_3 nano particles; (b) SAED of Cu and γ-Al_2O_3; (c) twins; (d) HRTEM image; (e) FFT of (e); (f) dislocation tangles.

formed by Cu and Zr. Gao et al. [50] prepared Cu-0.2 wt% Zr-0.15 wt% Y alloy, and identified a large amount of $Cu_{10}Zr_7$ phase generated in the Cu matrix through TEM analysis. Tian et al. [51] prepared Cu-1 wt%Zr alloy and found that the generated $Cu_{10}Zr_7$ phase can lead to lattice mismatch and increase the strength of the material, which plays an important role in strengthening the material. Due to various strengthening phases pinning dislocations and hindering their movement, dislocations entangle with each other in the Cu matrix, as shown in Fig. 5 (f). The entanglement of dislocations leads to an increase in the density of dislocations in the material, further strengthening the material.

3.2. Properties of composites

Table 2 shows the comprehensive properties of the two composites in the sintered state. The relative density of both Al_2O_3-Cu/25Cr1Zr and Al_2O_3-Cu/25Cr3Zr composites is above 98%. The conductivity of the two composite materials is 40.5 IACS% and 31.8 IACS%, respectively, and the hardness is 141HV and 154HV. Compared with pure copper, the conductivity decreases while the hardness increases. The decrease in conductivity is due to the distribution of Al_2O_3, Cr, and Zr particles generated by internal oxidation on the Cu matrix, causing lattice distortion and greatly increasing matrix defects, thereby increasing electron scatter. Moreover, the resistivity of Cr and Zr is much higher than Cu, which is the main reason for the decrease in electrical conductivity. Another important factor affecting electrical conductivity is the porosity of the material. The presence of pores hinders the movement of charges in the material, thereby reducing conductivity. The increase in hardness is due to the fact that the diffusely distributed Al_2O_3 and Zr particles in the Cu matrix pinch dislocations and cause dislocation entanglement buildup, which leads to an increase in the hardness of the composite. M. Ali et al. [52,53] prepared Cu-Ni/Al_2O_3 nanocomposites through in-situ synthesis. The in-situ generated Al_2O_3 was dispersed in the copper matrix, and the high bonding between the interface between the nano Al_2O_3 nanoparticles and the matrix was the main reason for the increase in material hardness and maintaining good conductivity.

Table 2
Comprehensive properties of Al_2O_3-Cu/(Cr, Zr) composites.

Composites	Electrical conductivity IACS%	Hardness HV	Actual density g/cm^3	Relative density %	Compressive strength MPa
Al_2O_3-Cu/25Cr1Zr	40.5	141	8.13	98.86	706
Al_2O_3-Cu/25Cr3Zr	31.8	154	8.06	98.59	815

During the process of electrical contact, collisions between moving and stationary contacts can cause bouncing and mechanical wear, and good wear resistance is one of the main performance requirements of electrical contact materials. The presence of in-situ generated nano Al_2O_3 particles, Cr and Zr particles in the Cu matrix increases the hardness of the composite material, making it difficult for the surface of the composite material to deform, thereby improving the wear resistance of the composite material [54,55]. In addition, the electrical contact material also needs to have high strength, and too low strength can lead to a decrease in the mechanical wear performance of the material, making it unable to meet certain specific service conditions [56]. Since it is more common for electrical contacts to be subjected to pressure during operation, room-temperature compression tests were performed on both composites. Fig. 6 shows the compression stress-strain curves of Al_2O_3 Cu/25Cr1Zr and Al_2O_3 Cu/25Cr3Zr composites. The compressive strength of Al_2O_3-Cu/25Cr1Zr and Al_2O_3-Cu/25Cr3Zr is 706 MPa and 815 MPa, respectively. The compressive strength increases by 15.4% with increased Zr content.

3.3. Mass change

Fig. 7 shows the mass change of the Al_2O_3-Cu/25Cr1Zr and Al_2O_3-Cu/25Cr3Zr composite materials after 10,000 opening and closing tests under 25 V DC and 10–40 A. It can be seen from Fig. 7(a) that the cathode mass of the Al_2O_3-Cu/25Cr1Zr composites decreases and the anode mass increases, which indicates that the material transfer direction is from the cathode to the anode during the electrical contact process. The decrease of the cathode mass is always larger than the increase of the anode mass, which suggests that there is part of the material loss splattering into the surroundings during the electrical contact process.

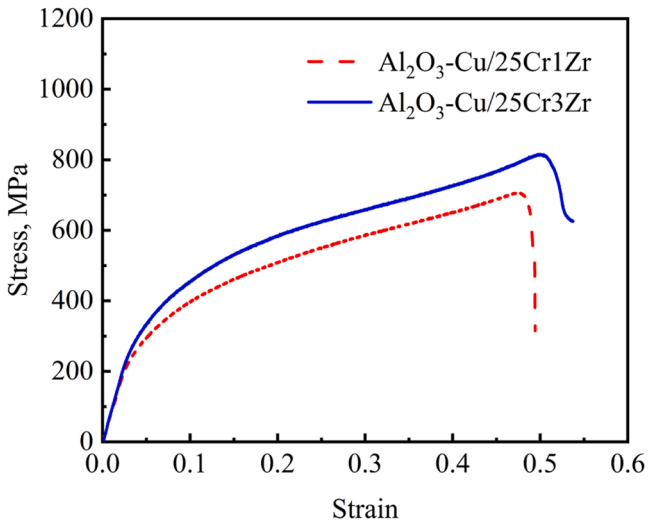

Fig. 6. Compressive stress-strain curves of composite materials.

When the current is 10 A, the mass transfer of the contact material is small because of the small current. With the increase of the current, the mass transfer of the material shows an increasing trend. It is worth noting that the change in the mass transfer of the electrical contact material is relatively small when the current rises from 20 A to 30 A, whereas there is a very large increase in the mass transfer of the material when the current increases from 30 A to 40 A. This phenomenon can be explained as follows. The mass transfer of electrical contact materials during the electrical contact process is the result of a combination of liquid bridge transfer, arc transfer, material gasification, and oxidation weight gain. Before the current is 30 A, the temperature of the electric contact is low, the melting gasification on the surface of the electric contact is less, and the transfer and loss of material are mainly realized through the arc transfer and a small amount of oxidation weight gain. When the current exceeds 30 A, the heating of the electrical contact intensifies, and the surface melting and evaporation are severe. At this time, the material transfer is not only through arc transfer and oxidation but also through liquid bridge transfer and material gasification. Therefore, a large amount of material splashes and evaporates into the surrounding environment during the opening and closing process of the electrical contact, exacerbating the mass transfer of the electrical contact material. The Al_2O_3-Cu/25Cr3Zr composite in Fig. 7(b) has a similar pattern of mass variation.

By comparing Fig. 7(a) and (b), it can be found that the quality change of the Al_2O_3-Cu/25Cr3Zr composite material is lower than Al_2O_3-Cu/25Cr1Zr under different current. As the Zr content increased from 1 wt% to 3 wt%, the mass transfer of the electrical contact material decreased by 14.2%, 28.5%, 27.2%, and 8.2% under 25 V DC and 10–40 A, respectively. This is because Zr has a high melting point and high-temperature stability. An increase in Zr content can effectively suppress the flow and splashing of molten Cu, reduce material mass transfer and loss to the surrounding environment, and improve the arc erosion resistance of the composite material.

3.4. Arc erosion morphology

Fig. 8 shows the SEM morphology of arc ablation of two kinds of composites under 25 V DC and 30 A. Fig. 9 shows the three-dimensional shape contour after arc erosion at 25 V DC and 30 A. After the electrical contact test, the contact surfaces are uneven and with significant changes. It can be seen that the surface of the anode is mainly composed of some protrusions, while the surface of the cathode shows some pits, which is consistent with the direction of mass transfer. It can also be seen from the three-dimensional morphology after arc ablation in Fig. 9 that with the increase in Zr content, the height of the anode's bulge decreases from 75 μm to 59 μm, and the depth of the cathode's pit decreases from 73 μm to 55 μm. This indicates that the resistance energy of the electrical contacts to arc ablation improves significantly with the Zr addition.

In order to observe the arc erosion morphology after electrical contact testing, higher magnification SEM observations were performed in Fig. 10. The surface of the electrical contact material forms typical arc erosion morphology such as bulges, droplets, holes, cracks, and liquid spreading. Due to the low melting point of Cu, it melts first at higher temperatures and splashes into the low-temperature zone during the contact closure and disconnection, forming droplets and protrusions seen in Fig. 10(a). Under the action of an arc, high temperatures are generated, and the metal on the surface of the electrical contact material melts to form a liquid spread. After the arc is ignited, it rapidly cools and solidifies, forming the morphology of the liquid spreading in Fig. 10(b). Cracks appear in Fig. 10(c), which due to the large difference in the thermal expansion coefficients between the Cu matrix and the two added Cr and Zr reinforcing phases, generating large thermal stresses during the liquid-solid transformation process and leading to cracks under the joint action of the contact force during the closure of the electrical contacts. In Fig. 10(c) a large number of gas holes and erosion pits are generated due to a large amount of gas dissolved in the molten pool during the arc erosion process. When the temperature decreases rapidly after the contact is disconnected, the metal liquid solidifies rapidly, and the dissolved gas will escape from it, resulting in a large number of gas holes. And the erosion potholes occur because when the arc energy is high, a jet flow occurs in the molten pool. During the jet flow process, liquid droplets splatter, leaving a "volcanic crater" like erosion pothole on the contact surface. The coral structure in Fig. 10(d) is due to the evaporation loss of Cu under high-temperature conditions, and the Cr and Zr with high melting points gradually gather and condense into a loose coral structure. Due to the evaporative loss of Cu under high-temperature conditions, Cr and Zr gradually aggregated and

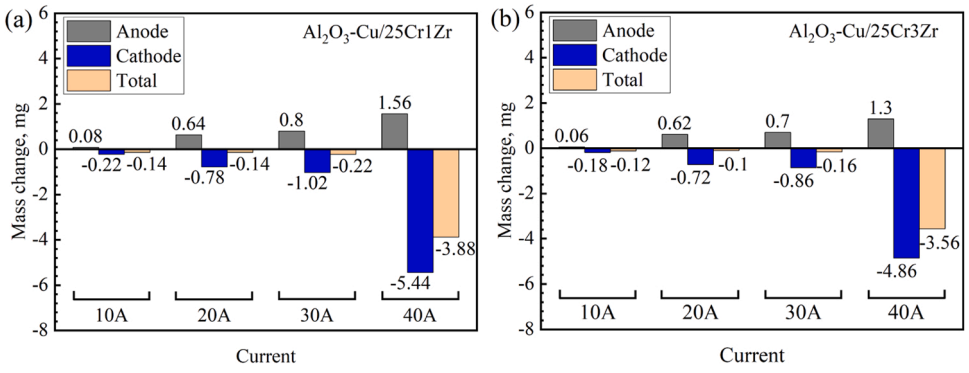

Fig. 7. Mass change of electrical contacts before and after electrical contact: (a) Al_2O_3-Cu/25Cr1Zr; (b) Al_2O_3-Cu/25Cr3Zr.

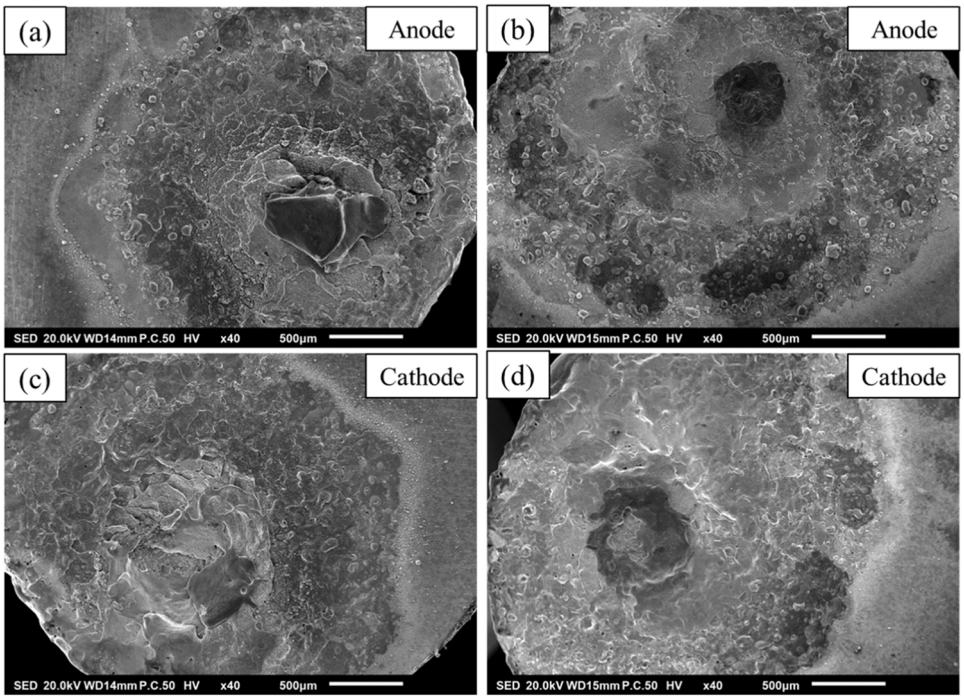

Fig. 8. SEM images of arc erosion morphology of electrical contacts at 25 V DC, 30 A: (a, c) Al_2O_3-Cu/25Cr1Zr; (b, d) Al_2O_3-Cu/25Cr3Zr.

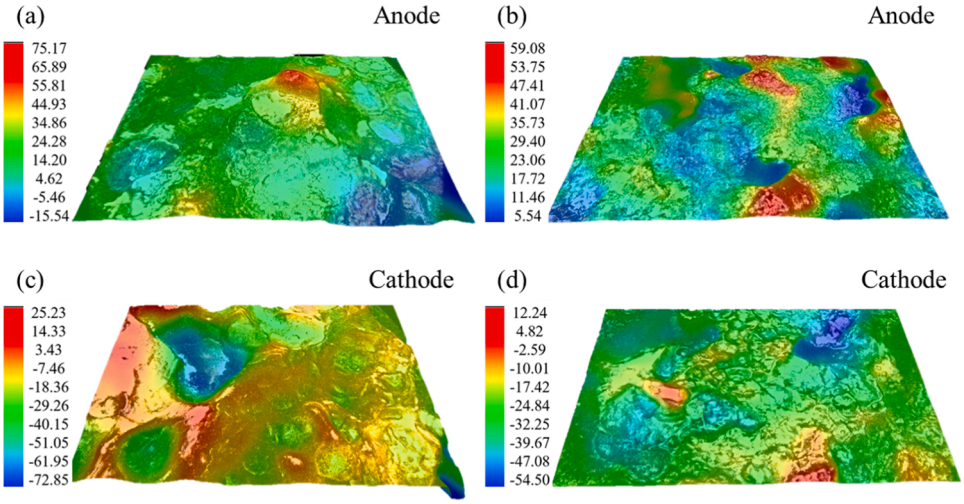

Fig. 9. Three-dimensional morphology of the surface of two kinds of electrical contacts after arc erosion at 25 V DC, 30 A: (a, c) Al_2O_3-Cu/25Cr1Zr; (b, d) Al_2O_3-Cu/25Cr3Zr.

condensed into the loose coral structure in Fig. 10(d).

The EDS results of the contact surfaces after arc ablation in Fig. 11 prove this further. Fig. 11(a) shows the SEM morphology and EDS surface scanning results of the eroded contact surface, and Fig. 11(b) shows the selected area EDS analysis of some typical arc ablation morphology. The surface protrusions and droplets are formed of melted and recondensed Cu. After melting at high temperatures, Cr and Zr recondense and distribute on the contact surface. In Fig. 11(b) the Cu content in the erosion pits produced in Region 1 is greatly reduced. There are some Cr or Cr oxides, and the small droplets in Region 2 are the Cu droplets formed after sputtering at high temperatures. Cr absorbs oxygen at high temperatures, forming small particles of chromium oxides in Region 3, and the main elemental compositions of the coral structure in Region 4 are Cr, O, and Zr.

3.5. *Welding force*

Fusion welding is the phenomenon of adhesive welding that occurs during the closing and opening of electrical contacts due to the melting of the contact surface caused by the arc heat flow. Electrical contacts are prone to failure due to fusion welding during contact. Therefore, electrical contact materials must also have good resistance to fusion welding [57]. Fig. 12 shows the changes in welding force of the Al_2O_3-Cu25Cr1Zr and Al_2O_3-Cu25Cr3Zr composites under 25 V DC, 10 A, and 40 A, with an average value taken for every 100 openings and closings. The fusion welding force of Al_2O_3-Cu25Cr1Zr and Al_2O_3-Cu25Cr3Zr composite materials at 10 A and 40 A conditions is 0.27–0.42 N and 0.32–0.57 N, respectively. The fusion welding force of both materials was relatively small, and they were able to consistently maintain good contact without fusion welding during the test. The welding force shows an increasing

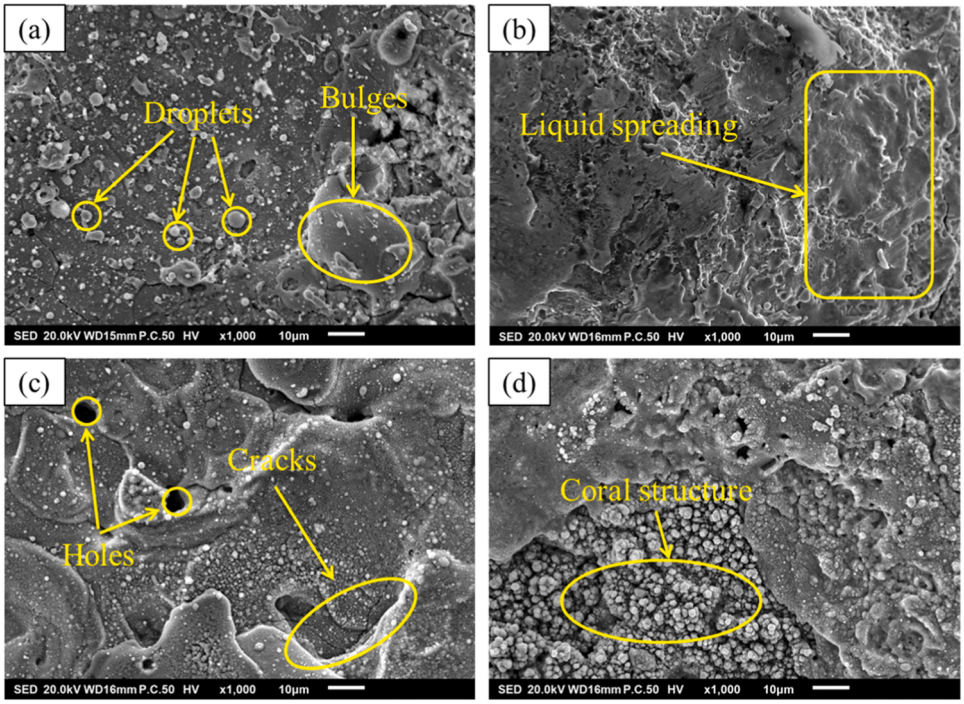

Fig. 10. SEM images of arc erosion morphology at 25 V DC, 30 A:(a) droplets and bulges; (b) liquid spreading; (c) holes and cracks; (d) coral structure.

trend as the current increases. At 40 A the fluctuation of welding force is very obvious, and it gradually increases with the number of contacts. This is because, at a fixed voltage, the electrical energy of the contact surface is converted into heat with increased current, which leads to the increase of Joule heat between the cathode and anode contacts. The wear of the electrical contact surfaces is more serious, the arc erosion is more obvious, and the heat generated between the electrodes will cause Cu to melt. When the contact is disconnected, the melted and cooled Cu will cause the contact surface of the two electrode contacts to stick, which will lead to an increase in the fusion welding force between the two electrodes. Under the same current, the fusion welding force of the Al_2O_3-Cu/25Cr1Zr composite is higher than the Al_2O_3-Cu/25Cr3Zr. For example, at 40 A, the average fusion welding force of Al_2O_3-Cu/25Cr1Zr and Al_2O_3-Cu/25Cr3Zr composites is 0.42 N and 0.33 N, respectively. This means that the average welding force decreased by 21.4% as the Zr content increased from 1 wt% to 3 wt%. The Al_2O_3-Cu/25Cr3Zr composites show better resistance to fusion welding.

3.6. Contact resistance

Contact resistance is the resistance generated by the cathode and anode electrical contacts after closure. Table 3 shows the average contact resistance of the Al_2O_3-Cu/25Cr1Zr and Al_2O_3-Cu/25Cr3Zr composites at 25 V DC and 10–40 A. The contact resistance is strongly related to the experimental parameters. At 25 V, the contact resistance of the Al_2O_3-Cu/25Cr1Zr and Al_2O_3-Cu/25Cr3Zr composites gradually decreases with current during the electrical contact process.

The magnitude and fluctuation of contact resistance are also related to the oxidation resistance of composites at the contact interface. Materials are prone to oxidation at the contact interface and the oxide film is prone to rupture, increasing the fluctuation of contact resistance. Under the same experimental conditions, the average contact resistance of the Al_2O_3-Cu/25Cr1Zr and Al_2O_3-Cu/25Cr3Zr materials does not vary much. In order to observe the changes in the closing resistance of the two materials more clearly, the variation of the closing resistance after 10,000 opening and closing times under 10 A and 20 A is plotted in Fig. 13. It can be observed that at 10 A, the contact resistance fluctuations of Al_2O_3-Cu/25Cr1Zr and Al_2O_3-Cu/25Cr3Zr materials are relatively small. When the current was increased to 20 A, the contact resistance of both Al_2O_3-Cu/25Cr1Zr and Al_2O_3-Cu/25Cr3Zr composites was relatively smooth for the first 5000 times, while the contact resistance of the two composites fluctuated significantly after 5000 cycles. The contact resistance of the Al_2O_3-Cu/25Cr3Zr composite is smaller, more stable, and less fluctuating than the Al_2O_3-Cu/25Cr1Zr composite. This is because Zr can improve the oxidation resistance, making it more difficult for the contact interface to oxidize during the electrical contact process.

3.7. Arc energy and arc duration

The arc energy and arc duration when the electrical contact is closed and disconnected is also an important indicator of the electrical contact material. They have a great influence on the mass change of the contact after arc erosion and the surface morphology. The longer the arc burning time, the higher the energy, the more serious the contact material heating, and the possibility of fusion welding will become larger, resulting in serious contact erosion. Fig. 14 shows the changes of average arc energy and average arc duration of the Al_2O_3-Cu/25Cr1Zr and Al_2O_3-Cu/25Cr3Zr electrical contact composites at 25 V DC, 10–40 A. When the current is low, the difference in average arcing time and energy between the two materials is not significant. However, as the current continues to increase, the average arcing time and energy of the two materials also gradually increase. The arcing time and arcing energy of the Al_2O_3-Cu/25Cr3Zr material are significantly lower than the Al_2O_3-Cu/25Cr1Zr. For example, when the current is 30 A, the average arc energy and average arc duration of Al_2O_3-Cu/25Cr3Zr are 20.1% and 28.1% lower than the Al_2O_3-Cu/25Cr1Zr, respectively. This shows that the increase of Zr can have a good effect of arc extinguishing.

4. Discussion

4.1. Relationship between arc energy and arc duration

It can also be seen from Fig. 14 that the arc energy and arc duration

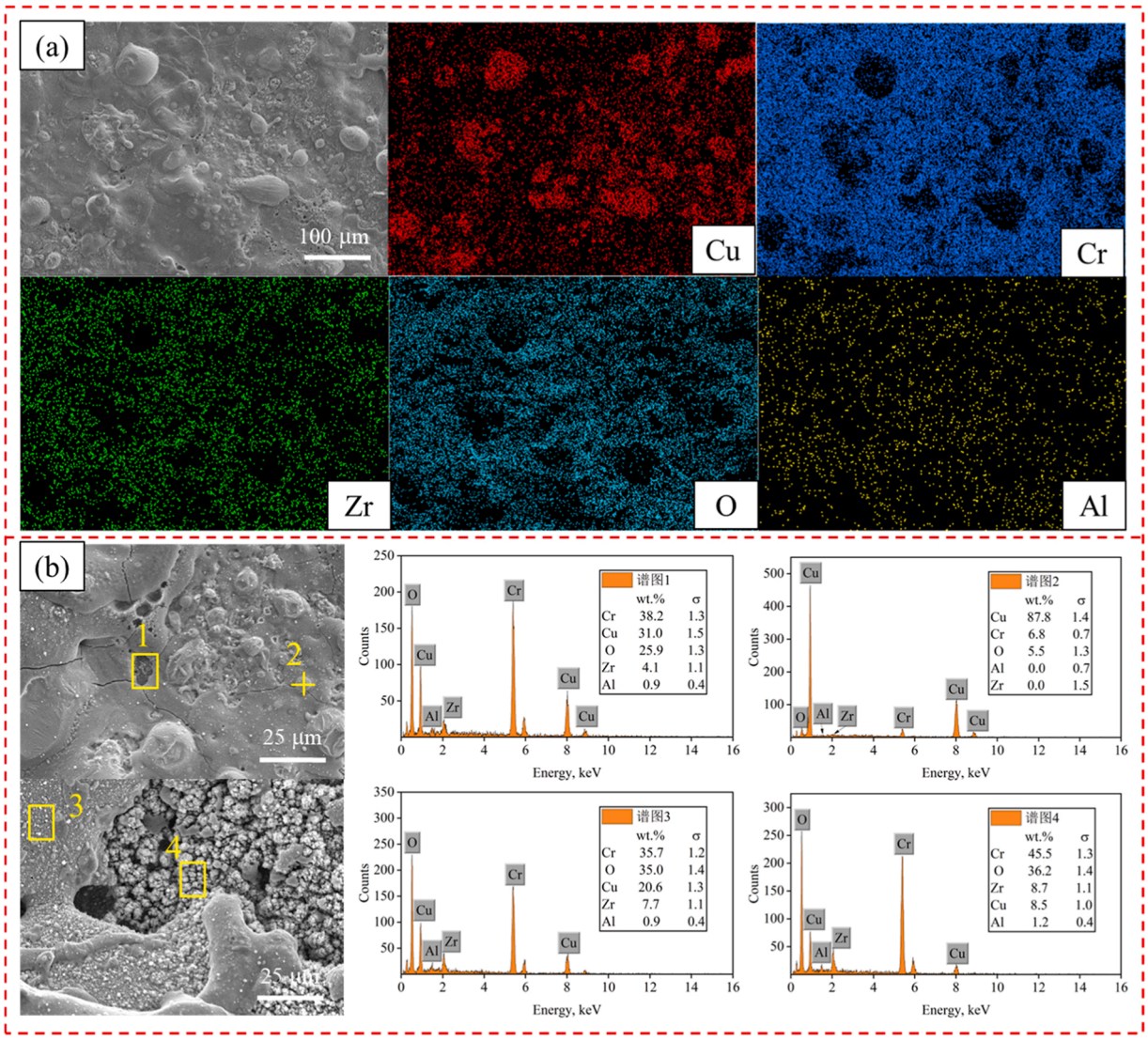

Fig. 11. EDS patterns of the surface of Al_2O_3-Cu/25Cr3Zr composite after 25 V DC, 30 A arc erosion:(a) EDS surface scanning; (b) EDS elemental analysis.

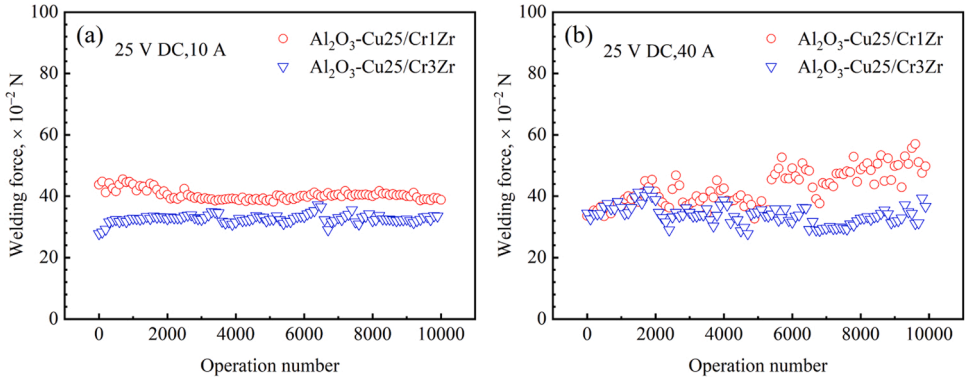

Fig. 12. Welding force of the Al_2O_3-Cu/25Cr1Zr and Al_2O_3-Cu/25Cr3Zr electrical contact composites under different currents. (a) 25 V DC, 10 A; (b) 25 V DC, 40 A.

of the two materials have similar trends. The data fitting of arc energy versus arc duration of the Al_2O_3-Cu/25Cr1Zr and Al_2O_3-Cu/25Cr3Zr composites were carried out at 25 V DC, 20 A and 30 A. The corresponding fitted equations are shown in Eqs. (2)–(5), and the corresponding R^2 is greater than 0.95, which indicates that the arc energy and arc duration during the electric contact process have a highly linear correlation.

$$E_1 = 71.48t_1\text{-}28.24 \quad R^2 = 0.992 \tag{2}$$

$$E_2 = 64.76t_2\text{-}7.63 \quad R^2 = 0.959 \tag{3}$$

Table 3
Contact resistance of the Al_2O_3-Cu/25Cr1Zr and Al_2O_3-Cu/25Cr3Zr composites.

Composites	Contact resistance, 10^{-3} Ω			
	10 A	20 A	30 A	40 A
Al_2O_3-Cu/25Cr1Zr	1.01	0.49	0.32	0.23
Al_2O_3-Cu/25Cr3Zr	0.98	0.47	0.31	0.23

$$E_3 = 87.74t_3 + 2.02 \quad R^2 = 0.956 \tag{4}$$

$$E_4 = 78.27t_4\text{-}34.06 \quad R^2 = 0.991 \tag{5}$$

where E_1, E_2, E_3, E_4 are the arc energy, and t_1, t_2, t_3, t_4 are the arc duration. Eq. (2) is the fitting equation of the Al_2O_3-Cu/25Cr1Zr composite at 25 V DC,20 A, Eq. (3) is the fitting equation of the Al_2O_3-Cu/25Cr3Zr composite at 25 V DC,20 A, Eq. (4) is the fitting equation of the Al_2O_3-Cu/25Cr1Zr composite at 25 V DC,30 A, Eq. (5) is the fitting equation of the Al_2O_3-Cu/25Cr3Zr composite at 25 V DC,30 A.

Fig. 15 shows the relationship between the arc energy and arc duration of the two composites at 25 V DC, 20 A and 30 A. From the Fig. 15, in the case of the same arc duration, the arc energy of Al_2O_3-Cu/25Cr3Zr is always lower than Al_2O_3-Cu/25Cr1Zr. For example, at points

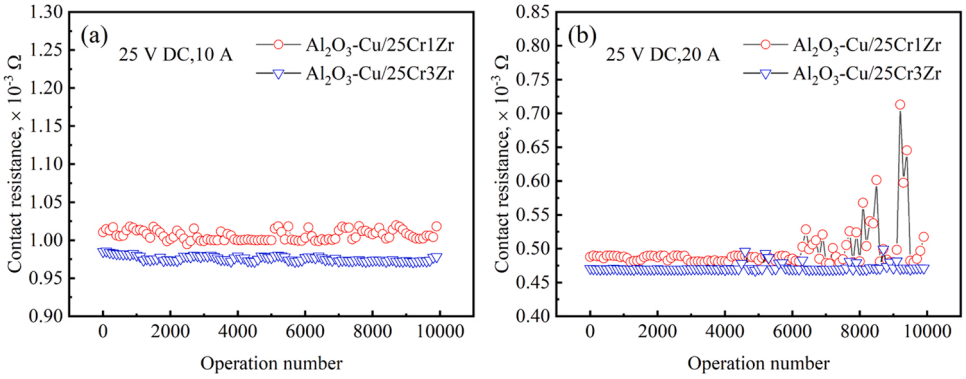

Fig. 13. Contact resistance changes of Al_2O_3-Cu/25Cr1Zr and Al_2O_3-Cu/25Cr3Zr electrical contact composites under different currents. (a) 25 V DC, 10 A; (b) 25 V DC, 20 A.

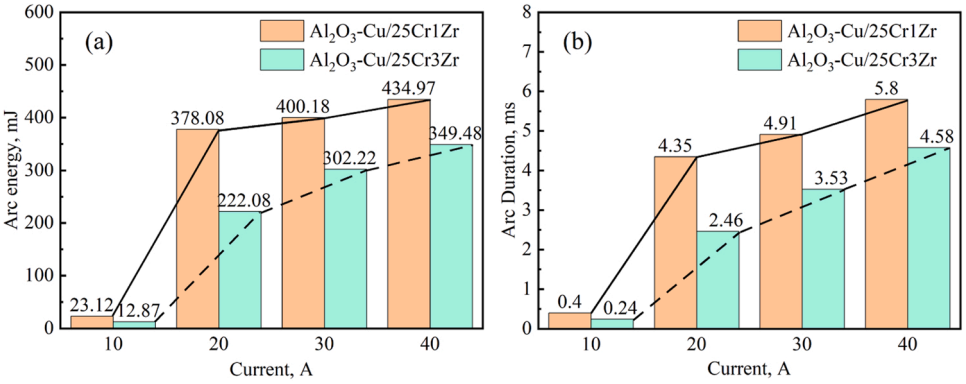

Fig. 14. Average arc duration and average arc energy of the Al_2O_3-Cu/25Cr1Zr and Al_2O_3-Cu/25Cr3Zr electrical contact composites under different current: (a) Average arc energy; (b) Average arc duration.

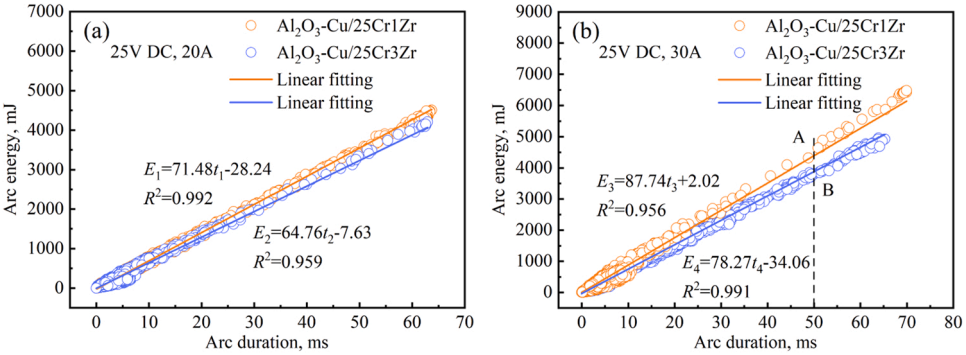

Fig. 15. Relationship between arc energy and arc duration for two composites. (a) 25 V DC, 20 A; (b) 25 V DC, 30 A.

A and B in the Fig. 15(b), the arc duration of the two materials is 50 ms, but the arc energy of Al_2O_3-Cu/25Cr3Zr is significantly lower than that of Al_2O_3-Cu/25Cr1Zr. With the same arc duration, the lower the arc energy, the less heat will be generated, and the erosion of the surface of the electrical contacts will be less severe with lower fusion welding probability.

4.2. Arc erosion mechanism

During the closing and opening process of the electrical contact, the temperature of the electrical contact increases due to arc discharge, and the low melting point Cu on the surface of the electrical contact melts and evaporates. The molten Cu forms droplets while boiling, and splashes and transfers during the closure and disconnection process of the electrical contact. Compared with Cu, Cr and Zr have higher melting points, which greatly limit the flow of Cu liquid and reduce the splashing of metal droplets. Arc erosion is a very complex process. Arc erosion can generate large protrusions and pits, leading to a decrease in contact area and thus damaging the connection of the circuit. This can lead to contact failure in severe cases [58], so it is necessary to explore the mechanism of arc erosion in composite materials.

Fig. 16 shows a schematic diagram of the material transfer of the arc erosion mechanism. The gas between the electrical contacts ionizes during contact closing or opening, leading to arc discharge, in turn, the formation of a molten bridge of liquid metal between the cathode and anode contacts. The heat flow and energy borne by the contact material will increase, and the temperature of the contact surface will rise sharply and then led to arc erosion. When the temperature of the contact surface rises to a certain extent, local materials will melt and adhere to the contact surface to form a molten pool. Then evaporation and splashing occur as the electrical contact closes and opens. The arc discharge will become more severe with increased current, leading to intensified material melting and accelerated diffusion of the material into the surrounding environment, even leading to explosive evaporation. In this process, the electrical contact material will be affected by the electron bombardment of the high-energy arc, electric field, electromagnetic force, and other factors. In order to maintain the arc stability, it is necessary to rely on the cathode to emit electrons. At this time, the cations between the arc column in the electric field force and the role of the electrons to accelerate the bombardment of the cathode contact surface. There will be many cations gathered at the cathode surface with the arc column dramatically shrinking at the cathode surface, ultimately leading to higher heat flow density of the cathode. The cathode heat is far greater than the anode, the material from the cathode to the anode and some of the transfer to the surrounding environment, resulting in material loss of material and unevenness of the electrical contact surface [59,60]. As the number of contacts increases, the area of the molten pool also increases, and the protrusions and pits on the surface also continue to increase. When the electrical contact is closed, the tip that first contacts will first generate an arc, and surface erosion will become more and more severe, ultimately leading to failure.

5. Conclusions

(1) Al_2O_3-Cu/25Cr1Zr and Al_2O_3-Cu/25Cr3Zr composite materials were prepared using internal oxidation and rapid hot pressing sintering methods. The relative density is above 98%, the conductivity is 40.5 IACS% and 31.8 IACS%, and the hardness is 141HV and 154HV, respectively. TEM analysis indicates that a large number of nano Al_2O_3 particles are dispersed on the copper matrix, strengthening the Cu matrix.

(2) After arc erosion, the anode and cathode surfaces were covered with bumps and pits, and the contact surfaces had a variety of sputtering droplets, holes, bulges, coral structures, and other types of arc erosion morphology. And the element distribution on the electrical contact surface changes significantly.

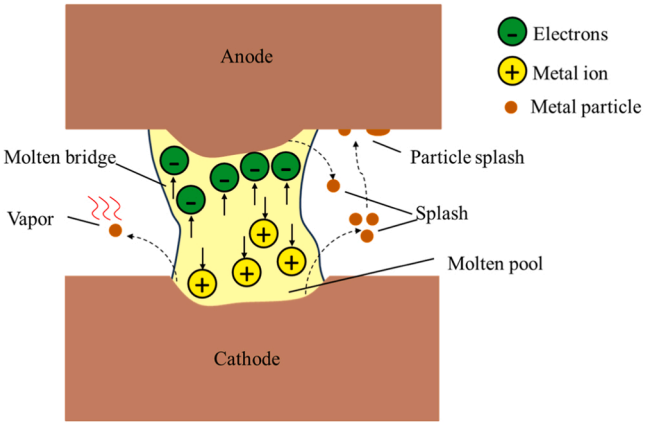

Fig. 16. The schematic diagram of the material transfer of the arc erosion mechanism.

(3) The mechanism of arc erosion during electrical contact is described. The material transfer direction is from the cathode to the anode during the electrical contact tests. Some materials were transferred to the surrounding environment, resulting in an increase in anode mass, a decrease in cathode mass, and a decrease in overall contact mass.

(4) Under the same experimental conditions, Al_2O_3-Cu/25Cr3Zr composite material exhibits better electrical contact performance. The increase in Zr significantly reduces mass transfer and loss during electrical contact, the arc duration and welding force are also significantly reduced, and the contact resistance is also more stable, which indicates that Zr improves the arc erosion resistance.

CRediT authorship contribution statement

Zhang YI: Funding acquisition, Writing – review & editing. **Li Xu:** Investigation. **Ma Zipeng:** Formal analysis. **Li Heng:** Conceptualization, Formal analysis, Methodology, Writing – original draft, Writing – review & editing. **Volinsky Alex A.:** Writing – review & editing. **Tian Baohong:** Resources, Supervision. **Zhou Meng:** Project administration, Resources. **Hu Haoyan:** Formal analysis. **Zou Jin:** Resources, Supervision. **Liu Yong:** Resources, Supervision. **Jing Ke:** Resources, Supervision.

Declaration of Competing Interest

The authors declare that they have no known competing financial interests or personal relationships that could have appeared to influence the work reported in this paper.

Data Availability

Data will be made available on request.

Acknowledgments

This work was supported by the National Natural Science Foundation of China (52071134), the Natural Science Foundation of Henan Province (232300420089), the Technology Innovation Center of Graphene Metrology and Standardization for State Market Regulation (AKYKF2309), the Program for Innovative Research Team at the University of the Henan Province (22IRTSTHN001), the China Postdoctoral Science Foundation (2023TQ0107), Key Research and Development Program of Jiangxi Province (20224BBE51047).

References

[1] O. Güler, T. Varol, Ü. Alver, A. Canakci, Effect of Al_2O_3 content and milling time on the properties of silver coated Cu matrix composites fabricated by electroless plating and hot pressing, Mater. Today Commun. 24 (2020), 101153.

[2] T. Varol, A. Canakci, E.D. Yalcin, Fabrication of nanoSiC-reinforced Al2024 matrix composites by a novel production method, Ara. J. Sci. Eng. 42 (5) (2017) 1751–1764.

[3] T. Varol, O. Güler, S.B. Akcay, H.C. Aksa, The effect of silver coated copper particle content on the properties of novel Cu-Ag alloys prepared by hot pressing method, Powder Technol. 384 (2021) 236–246.

[4] A. Fathy, M. Abdelhameed, F.A. Shehata, Effect of some manufacturing parameters on machining of extruded Al-Al_2O_3 composites, Int. Sch. Res. Not. (2012), 748734.

[5] A. Sergi, R.H.U. Khan, S. Irukuvarghula, M. Meisnar, A. Makaya, M.M. Attallah, Development of Ni-base metal matrix composites by powder metallurgy hot isostatic pressing for space applications, Adv. Powder Technol. 33 (2) (2022), 103411.

[6] G.H. Majzoobi, S.S. Jafari, K. Rahmani, A study on damage evolution in Cu-TiO2 composite fabricated using powder metallurgy followed by hot extrusion, Mater. Chem. Phys. 290 (2022), 126140.

[7] A. Azarniya, S. Sovizi, A. Azarniya, M.R.R.T. Boyuk, T. Varol, P. Nithyadharseni, H. R.M. Hosseini, S. Ramakrishna, M.V. Reddy, Physicomechanical properties of spark plasma sintered carbon nanotube-containing ceramic matrix nanocomposites, Nanoscale 9 (35) (2017) 12779–12820.

[8] O. Güler, T. Varol, Ü. Alver, G. Kaya, F. Yildiz, Microstructure and wear characterization of Al2O3 reinforced silver coated copper matrix composites by electroless plating and hot pressing methods, Mater. Today Commun. 27 (2021), 102205.

[9] H. Ahmadian, A.M. Sadoun, A. Fathy, T.F. Zhou, Utilizing a unified conceptual dynamic model for prediction of particle size of duel-matrix nanocomposites during mechanical alloying, Powder Technol. 418 (2023), 118291.

[10] A. Sadoun, A. Ibrahim, A.W. Abdallah, Fabrication and evaluation of tribological properties of Al_2O_3 coated Ag reinforced copper matrix nanocomposite by mechanical alloying, J. Asi. Ceram. Soc. 8 (4) (2020) 1228–1238.

[11] A.M. Sadoun, I.R. Najjar, G.S. Alsoruji, M.S. Abd-Elwahed, M.A. Elaziz, A. Fathy, Utilization of improved machine learning method based on artificial hummingbird algorithm to predict the tribological behavior of Cu-Al_2O_3 nanocomposites synthesized by in situ method, Mathematics 10 (8) (2022) 1266.

[12] Y. Fei, X.H. Wang, N.N. Zhao, H.Y. Li, Y.R. Qiu, Z. Li, Enhanced mechanical and electrical performance of Ag-4wt%ZrB_2 contact materials prepared with different-sized Ag powder, Mater. Today Commun. 37 (2023), 107104.

[13] S.C. Shu, Q. Zhang, J. Ihde, Q.L. Yuan, W. Dai, M.L. Wu, D. Dai, K. Yang, B. Wang, C. Xue, H.B. Ma, X. Zhang, J.M. Han, X.Y. Chen, C.T. Lin, W.B. Ren, Y.F. Ma, N. Jiang, Surface modification on copper particles toward graphene reinforced copper matrix composites for electrical engineering application, J. Alloy. Compd. 891 (2022), 162058.

[14] B.C. Yu, K.C. Bae, J.K. Jung, Y.H. Kim, Y.H. Park, Effect of heat treatment on the microstructure and wear properties of Al-Zn-Mg-Cu/In-Situ Al-9Si-SiCp/Pure Al composite by powder metallurgy, Met. Mater. Int. 24 (3) (2018) 576–585.

[15] J. Wang, Y.Q. Kang, C. Wang, Microstructure and vacuum arc characteristics of CuO skeletal structure Ag-CuO contact materials, J. Alloy. Compd. 686 (2016) 702–707.

[16] T. Kasagi, S. Yamamoto, Effect of particle shape on electrical conductivity and negative permittivity spectra of Cu granular composite materials, J. Mater. Sci. -Mater. Electron. 33 (8) (2022) 4974–4983.

[17] M. Demirtas, Microstructural, mechanical and tribological characterization of Cu-Co-Ni-Be alloy processed via equal channel angular pressing, Mater. Today Commun. 28 (2021), 102676.

[18] Y.Q. Qin, Y. Tian, Y.Q. Peng, L.M. Luo, X. Zan, Q. Xu, Y.C. Wu, Research status and development trend of preparation technology of ceramic particle dispersion strengthened copper-matrix composites, J. Alloy. Compd. 848 (2020), 156475.

[19] A.M. Sadoun, A. Fathy, Experimental study on tribological properties of Cu- Al_2O_3 nanocomposite hybridized by graphene nanoplatelets, Ceram. Int. 45 (18) (2019) 24784–24792.

[20] A.M. Sadoun, A.F. Meselhy, A.W. Abdallah, Microstructural, mechanical and wear behavior of electroless assisted silver coated Al_2O_3-Cu nanocomposites, Mater. Chem. Phys. 266 (2021), 124562.

[21] D. Saber, K. Abdelaziz, A. Fathy, Corrosion behavior of copper-alumina nanocomposites in different corrosive media, Int. J. Mech. Eng. 5 (6) (2016) 1–10.

[22] Y.Q. Qin, Y. Tian, Y. Zhuang, L.M. Luo, X. Zan, Y.C. Wu, Effects of solid-liquid doping and spark plasma sintering on the microstructure and mechanical properties of Y_2O_3-doped copper matrix composites, Vacuum 192 (2021), 110436.

[23] X.H. Zheng, M. Zhou, Y. Zhang, J.L. Huang, Y.Z. Li, H.J. Zhu, S.L. Tang, D. Li, S. L. Liang, B.H. Tian, Y. Liu, X. Li, Y.L. Jia, A.A. Volinsky, Microstructure and electrical contact behavior of Al_2O_3-Cu/30W3SiC(0.5 Y_2O_3) composites, J. Mater. Res. Technol. 22 (2023) 2158–2173.

[24] M. Elmahdy, G. Abouelmagd, A.A. Mazen, Microstructure and properties of Cu-ZrO_2 nanocomposites synthesized by in situ processing, Mater. Res. 21 (1) (2018), e20170387.

[25] A. Fathy, Investigation on microstructure and properties of Cu-ZrO_2 nanocomposites synthesized by in situ processing, Mater. Lett. 213 (2018) 95–99.

[26] M. Elmahdy, G. Abouelmagd, A.A. Mazen, Investigation on microstructure and thermal properties of in-situ synthesized Cu-ZrO_2 nanocomposites, Int. J. Mater. Res. 108 (12) (2017) 1103–1107.

[27] F. Shojaeepour, P. Abachi, K. Purazrang, A.H. Moghanian, Production and properties of Cu/Cr_2O_3 nano-composites, Powder Technol. 222 (2012) 80–84.

[28] X.H. Guo, K.X. Song, S.H. Liang, X. Wang, Y.M. Zhang, Effect of Al_2O_3 particle size on electrical wear performance of Al_2O_3/Cu composites, Tribol. Trans. 59 (1) (2016) 170–177.

[29] F. Shehata, M. Abdelhameed, A. Fathy, M. Elmahdy, Preparation and characteristics of Cu-Al_2O_3 nanocomposite, Open J. Metal. 1 (2011) 25–33.

[30] B.H. Tian, P. Liu, K.X. Song, Y. Li, Y. Liu, F.Z. Ren, J.H. Su, Microstructure and properties at elevated temperature of a nano- Al_2O_3 particles dispersion-strengthened copper base composite, Mater. Sci. Eng. A. 435–436 (2006) 705–710.

[31] H.J. Zhu, B.H. Tian, Y. Zhang, M. Zhou, Y.Z. Li, X.H. Zheng, S.L. Liang, S. Liu, W. Y. Sun, Y. Liu, A.A. Volinsky, Microstructure and electrical contact behavior of the nano-yttria-modified Cu- Al_2O_3/30Mo/3SiC composite, Nanotechnol. Rev. 12 (1) (2023).

[32] B. Li, G.M. Liu, J.H. Du, X.H. Zheng, Q.S. Yong, Study on the electrical arc ablation performance of Al_2O_3 reinforced Cu-matrix composites, Adv. Mater. Res. 557- 579 (2012) 267–271.

[33] R.J. Lin, L.J. Wang, J.W. Ma, W.X. Shi, J. Deng, S.L. Jia, Experiment investigation on vacuum arc of AMF contacts under different materials, Aip Adv. 8 (9) (2018).

[34] Y. Inada, R. Kikuchi, H. Nagai, A. Kumada, K. Hidaka, M. Maeyama, Influence of CuCr electrode composition on 2D electron and metal vapor density distribution over vacuum arc, J. Phys. D. 53 (30) (2020).

[35] S.X. Zhu, Y. Liu, B.H. Tian, Y. Zhang, K.X. Song, Arc erosion behavior and mechanism of Cu/Cr20 electrical contact material, Vacuum 143 (2017) 129–137.

[36] Y.J. Zhou, K.X. Song, J.D. Xing, Z. Li, X.H. Guo, Arc erosion behavior of Cu-0.23Be-0.84Co alloy after heat treatment: an experimental study, Acta Metall. Sin. 29 (4) (2016) 399–408.

[37] X.Y. Wan, W.B. Xie, H.M. Chen, F.Y. Tian, H. Wang, B. Yang, First-principles study of phase transformations in Cu-Cr alloys, J. Alloy. Compd. 862 (2021), 158531.

[38] K.Y. Duan, X.H. Guo, K.X. Song, X. Wang, J. Feng, S.L. Li, J.Y. Zhong, K. Li, Influence of WC particles addition on material transfer behavior of CuCr30 contact material, Mater. Today Commun. 34 (2023), 105058.

[39] D.V. Shangina, N.R. Bochvar, M.V. Gorshenkov, H. Yanar, G. Purcek, S. V. Dobatkin, Influence of microalloying with zirconium on the structure and properties of Cu-Cr alloy after high pressure torsion, Mater. Sci. Eng. A. 650 (2016) 63–66.

[40] N.T. Camara, R.A. Raimundo, C.S. Lourenco, L.M.F. Morais, D.D.S. Silva, R. M. Gomes, M.A. Morales, D.A. Macedo, U.U. Gomes, F.A. Costa, Impact of the SiC addition on the morphological, structural and mechanical properties of Cu-SiC composite powders prepared by high energy milling, Adv. Powder Technol. 32 (8) (2021) 2950–2961.

[41] X.H. Guo, Y.B. Yang, K.X. Song, S.L. Li, F. Jiang, X. Wang, Arc erosion resistance of hybrid copper matrix composites reinforced with CNTs and micro-TiB_2 particles, J. Mater. Res. Technol. 11 (2021) 1469–1479.

[42] X.H. Guo, K.X. Song, W. Xu, G.H. Li, Z.L. Zhang, Effect of TiB_2 particle size on the material transfer behaviour of Cu-TiB_2 composites, Mater. Sci. Technol. 36 (15) (2020) 1685–1694.

[43] W. Tian, L.M. Bi, F.C. Ma, J.D. Du, Effect of Zr on as-cast microstructure and properties of Cu-Cr alloy, Vacuum 149 (2018) 238–247.

[44] L.M. Bi, P. Liu, X.H. Chen, X.K. Liu, W. Li, F.C. Ma, Analysis of phase in Cu-15%Cr-0.24%Zr alloy, Trans. Nonferrous Met. Soc. 23 (5) (2013) 1342–1348.

[45] C. Watanabe, R. Monzen, K. Tazaki, Mechanical properties of Cu-Cr system alloys with and without Zr and Ag, J. Mater. Sci. 43 (3) (2008) 813–819.

[46] R.A. Mahdavinejad, M. Khajeafzali, Arc-erosion behavior of W/Zr/Cu electrical contact materials prepared by functionally graded composite technique, Met. Mater. Int. 27 (11) (2021) 4730–4741.

[47] X.H. Yang, J.T. Zou, P. Xiao, X.H. Wang, Effects of Zr addition on properties and vacuum arc characteristics of Cu-W alloy, Vacuum 106 (2014) 16–20.

[48] J.Q. Deng, X.Q. Zhang, S.Z. Shang, F. Liu, Z.X. Zhao, Y.F. Ye, Effect of Zr addition on the microstructure and properties of Cu-10Cr in situ composites, Mater. Des. 30 (10) (2009) 4444–4449.

[49] W.S. Barakat, M.I.A. Habba, A. Ibrahim, A. Fathy, O.A. Elkady, The effect of Cu coated Al_2O_3 particle content and densification methods on the microstructure and mechanical properties of Al matrix composites, J. Mater. Res. Technol. 24 (2023) 6908–6922.

[50] L.Q. Gao, X. Yang, X.F. Zhang, Y. Zhang, H.L. Sun, N. Li, Aging behavior and phase transformation of the Cu-0.2 wt%Zr-0.15 wt%Y alloy, Vacuum 159 (2019) 367–373.

[51] K. Tian, B.H. Tian, Y. Zhang, Y. Liu, A. Volinsky, Aging strengthening mechanism of the Cu-1.0Zr alloy, Metall. Mater. Trans. A. 48 (11) (2017) 5628–5634.

[52] M. Ali, A.M. Sadoun, G. Abouelmagd, A.A. Mazen, M. Elmahdy, Microstructure and mechanical characterization of Cu-Ni/Al_2O_3 nanocomposites fabricated using a novel in situ reactive synthesis, Ceram. Int. 48 (5) (2022) 6414–6422.

[53] M. Ali, A.M. Sadoun, M. Elmahdy, G. Abouelmagd, A.A. Mazen, Development and performance analysis of novel in situ Cu-Ni/ Al_2O_3 nanocomposites, Ceram. Int. 48 (16) (2022) 22672–22680.

[54] A.M. Sadoun, I.M.R. Najjar, A. Fathy, M.A. Elaziz, M.A.A. Al-qaness, A. W. Abdallah, M. Elmahdy, An enhanced Dendritic Neural Algorithm to predict the wear behavior of alumina coated silver reinforced copper nanocomposites, Alex. Eng. J. 65 (2023) 809–823.

[55] I.R. Najjar, I.R. Najjar, A. Fathy, A.W. Abdallah, A.W. Abdallah, M. Elmahdy, Prediction of tribological properties of alumina-coated, silver-reinforced copper nanocomposites using long short-term model combined with golden jackal optimization, Lubricants 10 (11) (2022) 277.

[56] X.H. Zhang, Y. Zhang, B.H. Tian, Y.L. Jia, M. Fu, Y. Liu, K.X. Song, A.A. Volinsky, X. Yang, H. Sun, Graphene oxide effects on the properties of Al_2O_3-Cu/35W5Cr composite, J. Mater. Sci. Technol. 37 (2020) 185–199.

[57] S.L. Liang, S. Liu, Y. Zhang, M. Zhou, B.H. Tian, Y.F. Geng, Y. Liu, Y.L. Jia, X. Li, A. A. Volinsky, Effect of in situ graphene-doped nano-CeO_2 on microstructure and electrical contact properties of Cu30Cr10W contacts, Nanotechnol. Rev. 10 (1) (2021) 385–400.
[58] S. Liu, L.H. Li, M. Zhou, S.L. Liang, Y. Zhang, J.L. Huang, B.H. Tian, Y.F. Geng, Y. Liu, Y.L. Jia, X. Li, A.A. Volinsky, Preparation and properties of graphene reinforced Cu/0.5$CeO_2$30Cr electrical contact materials, Vacuum 195 (2022).
[59] C.P. Wu, D.Q. Yi, W. Weng, S.H. Li, J.M. Zhou, Influence of alloy components on arc erosion morphology of Ag/MeO electrical contact materials, Trans. Nonferrous Met. Soc. 26 (1) (2016) 185–195.
[60] Y. Xi, X.H. Wang, Z.J. Zhou, H.Y. Li, X.H. Guo, Material transfer behavior of $AgTiB_2$ contact under different contact forces and electrode gaps, Trans. Nonferrous Met. Soc. 29 (5) (2019) 1046–1056.